Research Article Vol. 36, No. 4 / April 2019 / Journal of the Optical Society of America A B65

Journal of the Optical Society of America A

OPTICS, IMAGE SCIENCE, AND VISION

Computational simulation of human perception of spatially dependent patterns modulated by degree and angle of linear polarization

Gary P. Misson,[1,2,*] Shelby E. Temple,[3] and Stephen J. Anderson[1]

[1]School of Life and Health Sciences, Aston University, Birmingham, B4 7ET, UK
[2]South Warwickshire NHS Foundation Trust, Warwick Hospital, Lakin Road, Warwick, CV34 5BW, UK
[3]School of Biological Sciences, University of Bristol, Bristol, BS8 1TH, UK
*Corresponding author: g.misson@aston.ac.uk

Received 31 October 2018; revised 22 January 2019; accepted 23 January 2019; posted 23 January 2019 (Doc. ID 349663); published 22 February 2019

Recent studies on polarization perception have shown that humans are sensitive to patterned stimuli modulated by either angle of linear polarization (*AoP*) or degree of polarization (*DoP*). Here, we present a model of human polarization sensitivity that incorporates both *AoP* and *DoP* as spatially dependent input variables. Applying the model to both sinusoidal- and square-wave-modulated *DoP* and *AoP* inputs, we demonstrate the theoretical similarities and differences generated by such inputs. Our model indicates the following: (i) edge boundaries between two adjacent areas of different linear polarization are preserved for both *AoP*- and *DoP*-modulated stimuli; and (ii) compared with *DoP* stimuli, *AoP* stimuli generate greater luminance changes at the photoreceptor level, suggesting that *AoP*-modulated patterns are potentially more salient than *DoP* patterns. The computational model is supported experimentally with an optical test of the model comprising a radial diattenuating polarizing filter and modified liquid crystal displays generating *DoP*- and *AoP*-modulated outputs. Psychophysical measures of human sensitivity confirm the increased salience of *AoP*- relative to *DoP*-modulated stimuli. These findings have practical application to the selection of *DoP*- and *AoP*-modulated stimuli for the investigation of macular function and macular pigment density in healthy and diseased eyes.

https://doi.org/10.1364/JOSAA.36.000B65

1. INTRODUCTION

Humans are one of only a few vertebrate species with a well-documented ability to perceive polarized light [1–5]. Until recently, this was thought to be confined to the phenomenon of Haidinger's brushes (HB), the faint transient hour-glass-like pattern perceived in central vision when observing a uniform field of linear polarized white or blue light [1]. However, recent investigations using spatially modulated linear polarization fields have shown that humans are highly sensitive to angle of polarization (*AoP*) [6], even at a low degree of polarization (*DoP*) [7].

The human ability to perceive linear polarization relates directly to the radial structure of the macular retina and the diattenuating properties of carotenoid macular pigments [1]. This arrangement lends itself to computational modeling [8,9], and we recently published a model for a uniform linear polarized field that generated realistic simulations of HB [10].

The present study extends our previous work to include patterned linear polarization fields and *DoP*. In so doing, we are able to simulate the visual perception of patterned linearly polarized stimuli modulated either by *DoP* or *AoP*, scenarios that can be generated using liquid crystal display (LCD) technology [11]. Predictions arising from the model are tested using an optical model and *in vivo* measures on normally sighted human participants.

Cognizant that measures of polarization sensitivity may allow a targeted assessment of human macular function, we sought to determine which form of stimulus modulation—*AoP* or *DoP*—would provide the most sensitive measure of visual performance.

2. THEORY

The computations presented are based on a two-dimensional Stokes–Mueller representation of the polarization optics of the human eye (see [9,10,12] for details of the methods employed):

$$\mathbf{S}_{\mathbf{out}}[x, y, k_1, k_2] = D(x, y)\mathbf{M}_{\mathbf{M}}[x, y, k_1, k_2]\mathbf{M}_{\mathbf{dop}}[x, y]\mathbf{S}_{\mathbf{in}}[x, y]. \quad (1)$$

The current model includes degree of incident linear polarization represented by the Mueller matrix $\mathbf{M}_{\mathbf{dop}}[x, y]$ and a

non-uniform stimulus field represented by the input linear polarization Stokes vector $\mathbf{S_{in}}[x, y]$. As in the previous model [10], light passes through a radial diattenuating element modulated by a density function $D(x, y)$ that determines the spatial extent of the macular polarization sensitivity. All elements of the model are spatially dependent on a Cartesian coordinate system with its origin at the center of the macular radial diattenuator.

The model has been simplified by assuming radial symmetry of the polarization-sensitive components of the eye, and that the intrinsic ocular birefringence (principally, the cornea and macular retina) has no effect on the polarization state of light captured by photoreceptors. Furthermore, the photoreceptors are assumed to be insensitive to the polarization state of normally incident light. The justification for this has been discussed elsewhere [13].

Expressed in Cartesian coordinates with the origin at the fovea centralis (center of visual fixation), the light incident on photoreceptors after passing through the ocular structure and the radial macular diattenuator ($\mathbf{M_M}[x, y, k_1, k_2]$, with diattenuations k_1, k_2, is expressed as a transmission function derived from the first (intensity, S_0) component of the output Stokes' vector ($\mathbf{S_{out}}$):

$$T_M[x, y, k_1, k_2] = \frac{D(x, y)}{2}\left[(k_1 + k_2) + \frac{\begin{pmatrix} DoP(x, y)(k_1 - k_2)((x^2 - y^2)\cos(2AoP(x, y)) \\ +2xy\ \sin(2AoP(x, y)) \end{pmatrix}}{x^2 + y^2}\right], \tag{2}$$

where $DoP(x, y)$ $(0 \le DoP(x, y) \le 1)$ and $AoP(x, y)$ $(0 \le AoP(x, y) \le \pi)$ are functions that define, respectively, *DoP* and *AoP* of incident polarization at point (x, y). Both the *DoP* and *AoP* can be made spatially dependent (with an appropriate function or data array) or can be set as a constant value. For example, $DoP(x, y) = 1$ describes a polarization field that is everywhere 100% polarized; $AoP(x, y) = 0$ describes a polarization field that is everywhere horizontally linearly polarized. The pattern of spatially dependent *AoP* or *DoP* is given the term "base pattern."

Diattenuation, the dependence of the intensity transmittance of the exiting beam on the polarization state of the incident beam, is quantified by the orthogonal major (maximum) and minor (minimum) transmittances k_1, k_2, such that $0 \le k_2 < k_1 \le 1$. The orientations of k_1, k_2 are, respectively, radial and tangential about the central point of the system $(x = 0, y = 0)$, which corresponds to the center of the macula. If no extinction for polarized light parallel to the preferred orientation of the diattenuating elements $(k_1 = 1)$ is assumed [10], then a typical value is $k_2 = 0.88$, as determined from empirical data [14–16].

The density function $D(x, y)$ $(0 \le D(x, y) \le 1)$ describes the two-dimensional distribution of the region of the macula that absorbs polarized light, here assumed to correspond to the distribution and density of macular pigment. While several different patterns of macular pigment distribution have been described [17–19], a simple but physiologically realistic exponential model is used here (Sharifzadeh *et al.*'s [19] category "C"), defined as

$$D_1(x, y, \rho) = 10^{-\rho\sqrt{x^2+y^2}}, \tag{3}$$

where ρ is a constant. When $\rho = 0.3$, D is half the central (maximum) value at 1° eccentricity, and is undetectable from 6° to 8° [17]. Macular pigment density distributions or profiles are assumed to be radially symmetric. The second density function used in this study,

$$D_2(x, y, r) = \frac{1}{2}\left[1 + \mathrm{sign}\left(1 - \left[\left(\frac{x}{r}\right)^2 + \left(\frac{y}{r}\right)^2\right]\right)\right], \tag{4}$$

represents a disk (radius r) with uniform radial/tangential diattenuation surrounded by a non-diattenuating field, which is the theoretical equivalent of the radial diattenuator used in the optical evaluation described below.

While mathematically defined functions are used for *D*, *AoP*, and *DoP*, the model will accept any two-dimensional array of data, including graphics files.

3. METHODS

A. Simulation

Simulation of perceived images was performed using the two-dimensional radial diattenuator model [Eq. (2)] into which the density function [Eqs. (3), (4)] and appropriate expressions for the *DoP* and *AoP* functions have been substituted. Computational analyses and graphics generation were performed using Mathematica (Wolfram Research, Inc., Champaign, IL, Version 11.1.1.0, (2017)). The basic components of the simulations (density function, transmission functions for uniform fully polarized and depolarized fields) are shown in Fig. 1. The aim was to simulate *DoP*-modulated/*AoP*-constant or *AoP*-modulated/*DoP*-constant fields with stimuli used in typical psychophysical investigations, such as sinusoidal- and square-wave-modulated gratings and checkerboard patterns. These patterns were also used in the experimental verification of theory using a tangential diattenuating filter.

B. Optical Evaluation

As described previously [20], theory was tested in an optical model in which an LCD-generated polarization-modulated pattern was photographed through a polarizing filter with diattenuation that was radially symmetric about the center point of the filter (Oriel Instruments, "Polarization axis finder" 25328).

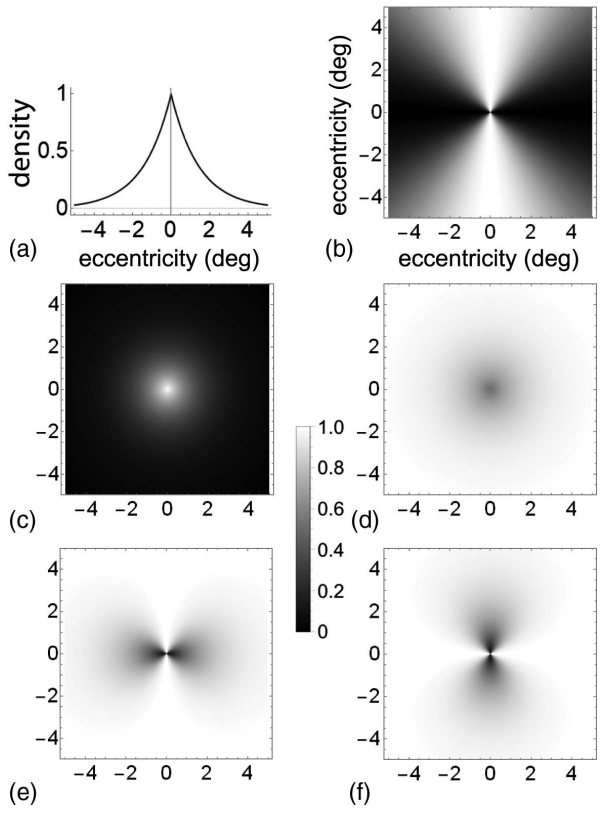

Fig. 1. Basic simulation components for a 5° × 5° field. (a) Plot of the density function D_1 relative to retinal eccentricity along the horizontal plane of a simulated macula with density ranging from 0 to 1, and following an exponential decline from center to periphery. (b) Two-dimensional representation of transmission function for fully ($DoP = 1.0$) polarized light oriented vertically ($AoP = \pi/2$ or 90°) as it passes through a perfect infinite radial diattenuator. (c) Two-dimensional representation of the density function D_1 as per (a). (d) Two-dimensional representation of the transmission function for depolarized ($DoP = 0$) light attenuated by density function D_1. (e) Two-dimensional representation of the transmission function for fully linearly polarized light with vertical orientation ($DoP = 1.0$, $AoP = \pi/2$). (f) Two-dimensional representation of the transmission function for fully linearly polarized light with horizontal orientation ($DoP = 1.0$, $AoP = 0$). Horizontal and vertical scales are degrees eccentricity from the center of the radial diattenuator (0, 0). The grayscale (0–1.0) indicates density for panel (c), and transmission for panels (b), (d), (e), and (f).

The method was extended here to two types of LCD: a twisted nematic (TN) LCD (Dell P1913Sb) for the generation of an *AoP* stimulus, and an in-plane switching (IPS) LCD (Dell P1914Sc) for the generation of a *DoP* stimulus [11]. Each of the monitors was converted into a polarization-modulated display by the removal of the front polarizing filter [7,21,22] and insertion of a blue-transmitting polymer filter (Lee Filters Ltd, UK, #075, "evening blue"; peak transmission 440–460 nm) behind the back polarizing filter of the LCD panel [6,20]. The luminance output of each monitor was the same, as determined using a photometer (model CS100-A, Minolta Co. Ltd., Japan); similarly, the spectral output of each monitor was identical, as determined using a solid-state spectrometer (USB2000, Ocean Optics Inc., FL, USA). The polarization output of the monitors was calibrated as previously described [6,11]. Densitometry of digital images was performed with image analysis software (Image J [23]).

C. *In Vivo* Evaluation

Human contrast thresholds for the detection of a three cycles per degree (cpd) grating for *AoP*, *DoP*, and luminance stimuli followed the experimental protocol of Misson and Anderson [6]. *AoP*- and *DoP*-modulated grating stimuli were generated using the modified TN and IPS LCD monitors described above. The luminance stimulus was provided by attaching a suitable polarizing filter to the front of the IPS LCD monitor. *DoP*, *AoP*, and luminance contrast threshold measures were determined using a modified version of the Freiburg Visual Acuity and Contrast Test (FrACT Version 3.9.822, [24,25]). LCD calibration determined the relationship between FrACT contrast values (C) and base image boundary differences in *AoP* (ΔAoP) and *DoP* (ΔDoP), such that $\Delta AoP = 0.85C - 1$ and $\Delta DoP = 0.0097C$. The monitors were orientated to give a horizontal/vertical *AoP* for a full contrast output ($C = 1$). Binocular contrast thresholds (CTs) were determined in five individuals ($M{:}F = 3{:}2$, age range 42–62 yrs) using a four-alternate forced-choice (4-AFC) paradigm with 36 trials per test run. The working distance was 1 m, and refractive errors were corrected for that distance with isotropic glass trial lenses. Testing was conducted under mesopic ambient lighting conditions (42 lux). All human experimentation followed the tenets of the Declaration of Helsinki and received local ethical approval.

4. RESULTS AND DISCUSSION

A. Simulation

The effect of pattern segmentation of polarization fields can be analyzed using discontinuous (square-wave) and continuous (sine-wave) two-cycle grating base patterns spanning the hypothetical observer field (Fig. 2). In each case, there is a uniform density function ($D = 1$); i.e., there is no superimposed spatially dependent constraint of the base pattern. Spatial modulation of *DoP* between 0 and 1 transforms the HB pattern in Fig. 1(b) into the images shown in Figs. 2(b) and 2(e) for sinusoidal and square-wave modulation, respectively. The corresponding changes for *AoP* modulation between horizontal and vertical ($AoP = 0, \pi/2$) are shown in Figs. 2(c) and 2(f). The difference between the images is clear for both discontinuous/continuous base pattern pairs and *DoP*/*AoP* pairs. Additional differences are noted with rotation of the incident polarization relative to the axes of the bars and with horizontal translations.

The discontinuous grating models are the simplest to quantify and most relevant to experimental evaluation, particularly *in vivo* [6,7,20]. Graphs of transmission along a horizontal profile ($y = 0$) show that maximum contrast across the polarization boundary occurs with *AoP* modulation [Fig. 2(h)] and is half this value with *DoP* modulation [Fig. 2(g)]. This follows from Eq. (2) solved for $DoP = 0$ when T_H is everywhere $(k_1 + k_2)/2$. For $DoP = 1$, Eq. (2) gives $T_H = k_1$ for $AoP = 0$ (horizontal) and $T_H = k_2$ for $AoP = \pi/2$ (vertical). It can also be deduced from Eq. (2) that for $AoP = \pi/4$ (45°, and any

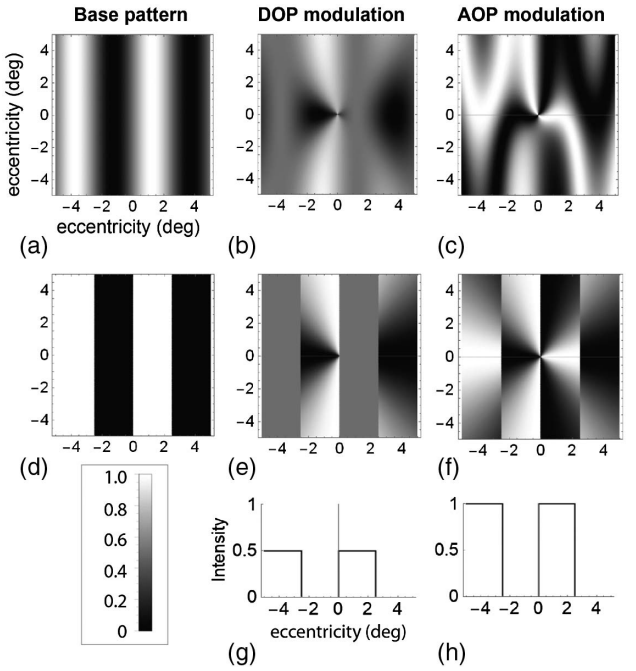

Fig. 2. Continuous (a)–(c) and discontinuous (d)–(f) two cycles per field grating simulations. Base patterns (a) (d) with *DoP* (b), (e) and *AoP* (c), (f) simulations for a perfect radial diattenuator ($k_1 = 0$, $k_2 = 0$). The density function was set at a constant value of 1. Scale (in box) is in fractions of $\pi/2$ for base patterns (a), (d) and relative intensity for simulations (b), (c), (e), (f). Figures (g) and (h) are relative intensity profiles along the x axis ($y = 0$) for the discontinuous grating simulations (e) and (f). All horizontal and vertical scales (a)–(f) are degrees eccentricity from the center of the radial diattenuator (0, 0). Vertical scales in (g) and (h) are intensity.

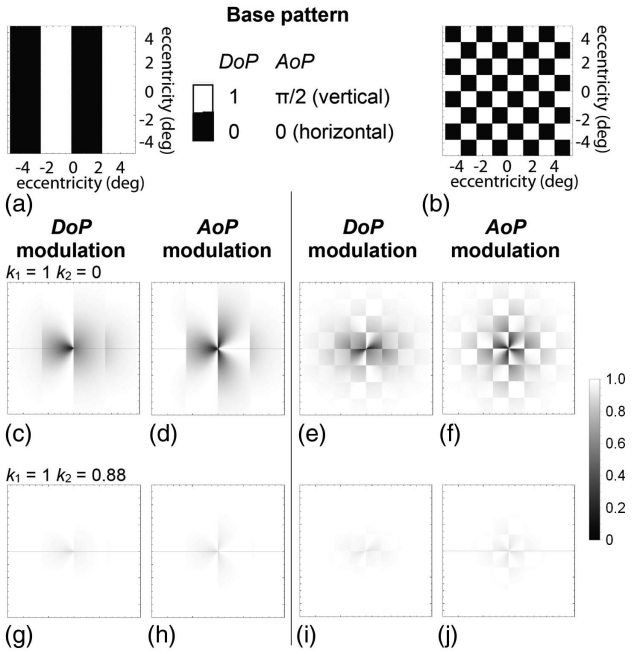

Fig. 3. Radial diattenuator simulations for a two-cycle per field grating (a) and a four-cycle per field checkerboard (b) base patterns for *DoP* and *AoP* modulation with a spatially modulated density function for a perfect diattenuator [$k_1 = 1$, $k_2 = 0$; (c)–(f)], and with physiological diattenuations [$k_1 = 1$, $k_2 = 0.88$; (g)–(j)]. Upper scale is *DoP* (0, 1) and *AoP* (0, $\pi/2 = 90°$) for base patterns (a), (b); scale to the right provides relative transmission for plots (c)–(j). The center of each plot (c)–(j) is the center of the radial diattenuator.

odd multiple thereof) $T_H = (k_1 + k_2)/2$, which is the same as that for depolarized light [i.e., there will be zero contrast across a grating boundary when one side is fully linearly polarized with an *AoP* of 45° and the other side is either orthogonally fully polarized (–45°) or fully depolarized]. Maximum transmission intensity difference ($k_1 - k_2$) is achieved across a linear boundary with both sides fully polarized, one side with *AoP* parallel to the boundary (k_1), the other side with *AoP* orthogonal to the boundary (k_2). Across a similar boundary, but with one side fully depolarized, the transmission intensity difference is half this value [$(k_1 - k_2)/2$].

The effect of introducing the density function D_1 [Eq. (3)] on the simulations shown in Figs. 2(e) and 2(f) are shown in Figs. 3(c) and 3(d), respectively, for a perfect diattenuator, and in Figs. 3(g) and 3(h), respectively, for physiological diattenuations. An additional set of simulations for a four-cycle per field checkerboard base pattern [Figs. 3(b), 3(e), 3(f), 3(i), 3(j)] demonstrates the differences in salience of the simulated percepts and the application of the model to a checkerboard base pattern.

B. Optical Model

Digital images of the effect of observing *DoP*- and *AoP*-modulated patterns through the radial diattenuating polarizing filter are shown in Figs. 4 and 5, where they are compared with the relevant simulations for a radial diattenuating disk (density function D_2). Diattenuations of $k_1 = 0.87$, $k_2 = 0.08$ can be estimated from digital densitometry along the horizontal line shown in the experimental images in Fig. 4. A close agreement with the theoretical values can be seen both in this figure and in Fig. 5 for a checkerboard base pattern.

C. *In Vivo* Human Results

CTs for the detection of a 3 cpd square-wave grating, averaged across five participants, for both *AoP* (mean = 11.7% ± sem = 3.5%) and *DoP* (26.9% ± 6.1%) are shown in Fig. 6. These values correspond to $\Delta AoP = 9° \pm 2°$ and $\Delta DoP = 0.26 \pm 0.06$. Note that the luminance CT was less than the experimental FrACT instrumental resolution limit of 0.51% for all participants, and is plotted here as equal to 0.51%. Note also that the *DoP* CT was approximately double the *AoP* threshold, as predicted from our model.

5. GENERAL DISCUSSION AND CONCLUSION

Previous models of human polarization sensitivity are limited to observed polarization fields that are fully linearly polarized (*DoP* = 1). A recent model generated realistic simulations of HB by including diattenuation parameters and a density distribution representing the area of retina interacting with the polarized component of incident light [10]. The model developed in this study progresses further to simulate the perception of patterned polarization stimuli by including both *DoP* and

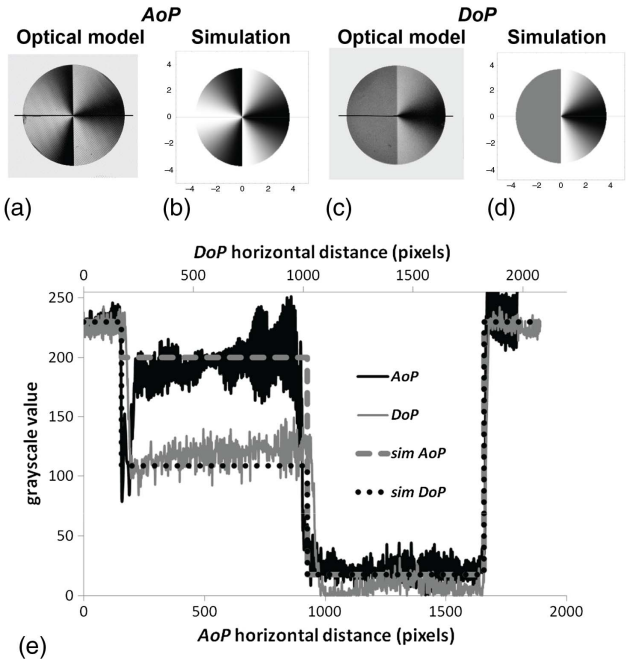

Fig. 4. Optical model evaluation. Radial diattenuating filter photographed in front of: (a) TN LCD generating orthogonal states of linear polarization (left half vertical, right half horizontal) compared with simulation shown in (b). (c) IPS LCD generating *DoP* of zero (left half) and *DoP* = 1 horizontal, linear polarized light (right half) compared with simulation shown in (d). (e) Density profiles along horizontal line in images (a) and (c) (*AoP* continuous black line; *DoP* continuous gray line) compared with corresponding theoretical predictions (simulated *AoP* dashed gray line; simulated *DoP* dotted black line). Transmission through the depolarized hemifield is half the difference in transmission between orthogonally polarized hemifields. The background of the optical model images is polarized according to the base function, but appears uniform as the camera is polarization insensitive, and there is no change in luminance of the patterned polarization fields.

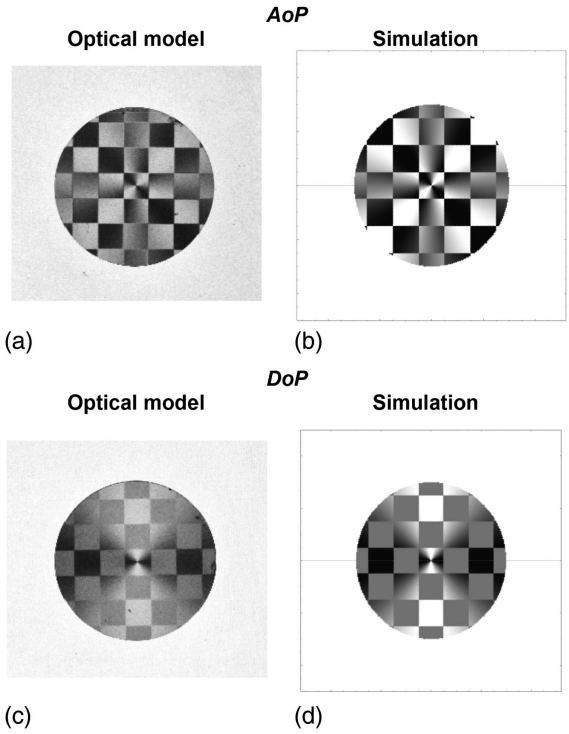

Fig. 5. Agreement between experimental results of the radial diattenuating filter on an *AoP* (a) and *DoP* (c) background compared with corresponding simulations (b), (d) for a radially diattenuating disk defined by density function D_2. The *AoP* background (a) is a TN LCD generating orthogonal states of linear polarization (±45°). The *DoP* background (c) is an IPS LCD generating *DoP* of zero and *DoP* = 1, *AoP* = 0°.

AoP observed fields that can be spatially modulated by a chosen base pattern.

The model is used for the first time to simulate the perception of both sinusoidally modulated (continuous) and square-wave-modulated (discrete) *AoP* and *DoP* fields. The resulting simulations have markedly different characteristics. As expected, a continuously variable base pattern generates a corresponding continuous simulation that is geometrically different for *AoP* compared with *DoP* [e.g., compare Figs. 2(b) and 2(c)]. This difference is also seen in the discontinuous base pattern, where an additional property of edge preservation for both *AoP* and *DoP* fields is observed [Figs. 2(e)–2(f); Figs. 3–5), thus extending a previous finding for *AoP* fields [20] to *DoP* fields. Edge preservation was the rationale for using discontinuous base pattern *AoP* stimuli in recent *in vivo* studies [6].

Computational modeling revealed that the simulated maximum contrast of *AoP* stimuli is twice that of *DoP* stimuli. This has practical implications in that, for a given base pattern, *AoP* modulation is a potentially stronger physiological stimulus than *DoP* modulation. This suggests a different potential role for each stimulus type. As *AoP* stimuli are the most salient, they may provide a more robust test of polarization vision in clinical measures of normal and abnormal macular function. *DoP* stimuli, on the other hand, may provide a more sensitive

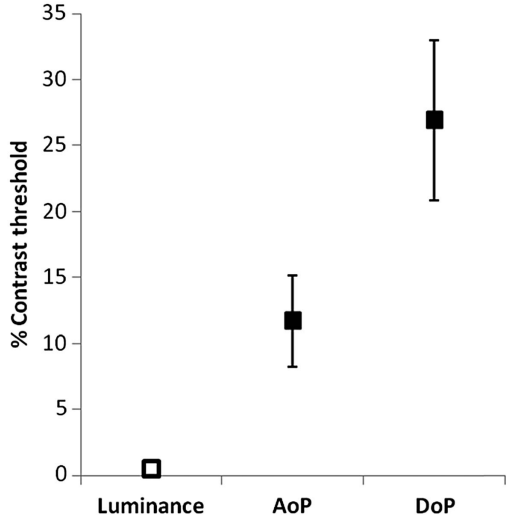

Fig. 6. Mean (± one SEM) luminance, *AoP* and *DoP* contrast thresholds for the detection of a 3 cpd grating stimulus. Note that for all participants, the luminance contrast threshold (open symbol) was less than the experimental resolution limit of 0.51% (see text).

measure of the physiological variation in a given parameter in normal eyes, such as macular pigment density [7].

Simulation predictions were verified in an optical model comprising a radially diattenuating polarizing filter and LCDs that generate both *AoP* and *DoP* patterned fields (Figs. 4 and 5). This study introduces modified IPS LCDs as a convenient source of *DoP* fields for both *ex vivo* and *in vivo* exploration of human polarization perception.

We further demonstrated that humans are able to detect spatially modulated *DoP* and *AoP* fields with CTs equivalent to a difference in *DoP* of 0.26 and a difference in *AoP* of 9°. These results are comparable with those of previous studies [6,7] and confirm that humans have a high degree of polarization sensitivity. Consistent with our theoretical model, the measured *DoP* CT was approximately twice that of the measured *AoP* threshold, when the same base pattern was used (see Fig. 6). The human visual system is, therefore, approximately twice as sensitive to an *AoP* stimulus than a *DoP* stimulus of the same base pattern. The threshold for the same base pattern in luminance contrast is lower by at least an order of magnitude, indicating that both *AoP* and *DoP* stimuli are relatively weak compared with luminance-modulated patterns.

A limitation of the present model is that it does not include ocular retardation. While this may have a confounding effect on quantitative measurements in individuals with high magnitudes of corneal retardation, it appears unlikely to be a significant factor in most individuals [10].

In conclusion, we describe a widely applicable model of human polarization sensitivity that can be applied to spatially modulated *AoP* and *DoP* fields. Differences in predicted simulations between *AoP* and *DoP* fields are confirmed in an optical model and *in vivo*. We show, for the first time, that normal humans are at least twice as sensitive to *AoP*-modulated patterns as they are to *DoP*-modulated patterns.

Funding. Innovate UK (900042).

REFERENCES

1. J. McGregor, S. E. Temple, and G. Horváth, "Human polarization sensitivity," in *Polarized Light and Polarization Vision in Animal Sciences*, G. Horváth, ed., 2nd ed. (Springer, 2014), pp. 303–315.
2. S. Akesson, "The ecology of polarization vision in birds," in *Polarized Light and Polarization Vision in Animal Sciences*, G. Horváth, ed., 2nd ed. (Springer, 2014), pp. 275–292.
3. V. B. Meyer-Rochow, "Polarization sensitivity in amphibians," in *Polarized Light and Polarization Vision in Animal Sciences*, G. Horváth, ed., 2nd ed. (Springer, 2014), pp. 249–263.
4. N. W. Roberts, "Polarization vision in fishes," in *Polarized Light and Polarization Vision in Animal Sciences*, G. Horváth, ed., 2nd ed. (Springer, 2014), pp. 225–247.
5. V. B. Meyer-Rochow, "Polarization sensitivity in reptiles," in *Polarized Light and Polarization Vision in Animal Sciences*, G. Horváth, ed., 2nd ed. (Springer, 2014), pp. 265–274.
6. G. P. Misson and S. J. Anderson, "The spectral, spatial and contrast sensitivity of human polarization pattern perception," Sci. Rep. **7**, 16571 (2017).
7. S. E. Temple, J. E. McGregor, C. Miles, L. Graham, J. Miller, J. Buck, N. E. Scott-Samuel, and N. W. Roberts, "Perceiving polarization with the naked eye: characterization of human polarization sensitivity," Proc. R. Soc. B **282**, 20150338 (2015).
8. G. P. Misson, "Form and behaviour of Haidinger's brushes," Ophthal. Physiol. Opt. **13**, 392–396 (1993).
9. G. P. Misson, "A Mueller matrix model of Haidinger's brushes," Ophthal. Physl. Opt. **23**, 441–447 (2003).
10. G. P. Misson, S. E. Temple, and S. J. Anderson, "Computational simulation of Haidinger's brushes," J. Opt. Soc. Am. A **35**, 946–952 (2018).
11. J. J. Foster, S. E. Temple, M. J. How, I. M. Daly, C. R. Sharkey, D. Wilby, and N. W. Roberts, "Polarization vision: overcoming challenges of working with a property of light we barely see," Naturwissenschaften **105**, 27 (2018).
12. R. W. Knighton and X. R. Huang, "Linear birefringence of the central human cornea," Invest. Ophthalmol. Vis. Sci. **43**, 82–86 (2002).
13. N. W. Roberts, H. F. Gleeson, S. E. Temple, T. J. Haimberger, and C. W. Hawryshyn, "Differences in the optical properties of vertebrate photoreceptor classes leading to axial polarization sensitivity," J. Opt. Soc. Am. A **21**, 335–345 (2004).
14. R. A. Bone, "The role of the macular pigment in the detection of polarized light," Vision Res. **20**, 213–220 (1980).
15. R. A. Bone and J. T. Landrum, "Distribution of macular pigment components, zeaxanthin and lutein, in human retina," Methods Enzymol. **213**, 360–366 (1992).
16. J. M. Bueno and P. Artal, "Average double-pass ocular diattenuation using foveal fixation," J. Mod. Opt. **55**, 849–859 (2008).
17. J. B. R. Hammond, B. R. Wooten, and D. M. Snodderly, "Individual variations in the spatial profile of human macular pigment," J. Opt. Soc. Am. A **14**, 1187–1196 (1997).
18. P. S. Bernstein, F. C. Delori, S. Richer, F. J. M. van Kuijk, and A. J. Wenzel, "The value of measurement of macular carotenoid pigment optical densities and distributions in age-related macular degeneration and other retinal disorders," Vision Res. **50**, 716–728 (2010).
19. M. Sharifzadeh, P. S. Bernstein, and W. Gellermann, "Nonmydriatic fluorescence-based quantitative imaging of human macular pigment distributions," J. Opt. Soc. Am. A **23**, 2373–2387 (2006).
20. G. P. Misson, B. H. Timmerman, and P. J. Bryanston-Cross, "Human perception of visual stimuli modulated by direction of linear polarization," Vision Res. **115**(Part A), 48–57 (2015).
21. R. M. Glantz and J. P. Schroeter, "Polarization contrast and motion detection," J. Comp. Physiol. **192**, 905–914 (2006).
22. V. Pignatelli, S. E. Temple, T.-H. Chiou, N. W. Roberts, S. P. Collin, and N. J. Marshall, "Behavioural relevance of polarization sensitivity as a target detection mechanism in cephalopods and fishes," Philos. Trans. R. Soc. B **366**, 734–741 (2011).
23. C. A. Schneider, W. S. Rasband, and K. W. Eliceiri, "NIH Image to ImageJ: 25 years of image analysis," Nat. Methods **9**, 671–675 (2012).
24. M. Bach, "The Freiburg visual acuity test-variability unchanged by post-hoc re-analysis," Graefe's Archive for Clin. Exp. Ophthalmol. **245**, 965–971 (2007).
25. M. Bach, "Freiburg vision test ('FrACT')," 2014, http://michaelbach.de/fract/.